Molybdenum rods assembled with nanosheets: a high catalytic material for phenol sensing

Rizwan Wahab [a, *], Farheen Khan [b], Naushad Ahmad [c], Manawwer Alam [c]

[a] Zoology Department, College of Science, King Saud University, Riyadh 11451, P.O.Box 2455, Saudi Arabia
[b] Chemistry Department, Faculty of Science, Taibah University, Madina, Yanbu, 42353, Saudi Arabia
[c] Department of Chemistry, College of Science, King Saud University, Riyadh 11451, P.O. Box 2455, Saudi Arabia

ABSTRACT

The phenol (PhOH) is a toxic chemical and can affect to the environment and human directly and indirectly. Due to their toxic nature it is listed as a carcinogenic compound for human health. The sensitivity of the PhOH in liquid medium can be detemine through various techniques in liquid medium was detected through various techniques for instance HPLC, mass, fluorescence and spectrophotometry etc but all of these techniques are expensive and not easily available to detect the longer range of samples in a very less time. To keep this view the present manuscript was designed to shows the utilization of metal oxide nano and microstructures as sensor material, therefore, initially highly crystalline molybdenum oxide rods assembled with nanosheets (referred to as α-MoO₃ RANs) was synthesized via solution process and utilized for sensing against PhOH. The α-MoO₃RANs exhibit numerous applications in various directions such as catalyst, LEDs, Field emission devices, batteries etc. The α-MoO₃RANs were formed from the solution processes in a short time span. The formed powder was well characterized through the techniques such as XRD, SEM, TEM and FTIR. From the analysis, it reveals that the size of each NS is ~200 nm in diameter whereas rods shaped structures length goes to 2−6 μm with good structural and chemical characteristics. The crystalline α-MoO₃RANs were applied for the electro chemical studies as three electrode system (GCE as working electrode, Ag/AgCl as reference and pt wire as counter electrode) with PhOH as an analyte in PBS. The electrochemical studies were conducted through cyclic voltammetry (CV) in terms of their low to high conc-entration ranges from 7.8 to 1000 μM in PBS, scan rate at different potential from 5 to 100 mV with the α-MoO₃RANs based working electrode (α-MoO₃RANs/GCE). The designed working electrode sensor having excellent reproducibility, sustained in presence of 62.25 μM (PhOH) for seven consecutive cycles. Including this, the chronoamperometry (0 −1500s) and electrochemical impedance spectra (EIS) were also analyzed. A probable mechanism was also discussed based on the analysis and their observations.

© 2020 Elsevier Ltd. All rights reserved.

1. Introduction

The clean and safe environment is a great concern in the community for the health and security purposes in the current scenario. The semiconductor materials, which are largely utilized in detoxification of environment with a well-organized technique. To control this, the small scale nano and microstructures are very efficient and exhibit an exceptional properties for instance larger surface to volume rations, organized geometry, facilitates to adsorb and absorbed the surfaces of toxic chemical also responsible to degradate the larger molecular weight organic chains. With these properties, the oxide based metal-oxide nanostructures exhibit a great concern due to their excellent standards such as higher porosity value, easy formation process, good quantum confinement effect, and larger stability at high temperature etc [1,2]. Enroute of this, the nano-carbons, which have an excellent bio-sensing activity against to detect the bacteria and it can be utilized the nano-carbons materials as a nanodevice for next generation [3]. The nano-carbon based sensing devices have capability to produce fast, efficient, profound, precise detection of bacterial cells, which could replace the complex procedures [3]. In continuation to this, recently the Graphene sheets have enormous attention due to their excellent properties such as high surface-to-volume ratio, excellent

conductivity, and high electron transpiration, which provides new stage of sensing and graphene-based sensors are utilized for the detection of volatile organic compounds (VOCs) to diagnose various types of diseases [4]. Based on the morphology, doping and surface modification, atomic scale organization, and various shaped nanostructured materials exhibit gas sensing properties and provides opportunities for further developments and applications in different fields [5]. The polymeric materials, which exhibit high flexibility with a wide range of applications such as in flexible electronics, transducers, lithium ion batteries and other various biomedical applications including self-healing property in human organs [6]. Although, polymeric material provides various applications in different directions but it has long processing conditions and needs various complexing agents. The single and conjugated oxide based materials are largely used to sense the hazardous chemicals also to enable to monitor the air and water pollution in the environment. The sense and elimination of toxic compounds from the industrial waste water is one of the crucial issues in the environmental and health prospects. Over various industrial hazardous compounds the toxicity assessment of PhOH and their derivatives in normal water, discharged effluents are exhibit major significance and envisioned for environmental management and safety [7,8]. The derivatives of PhOH or their related compound's having toxic impact on human, animals, and plants. These compounds provide unsolicited taste, and odor for the consumption of water, even at very trace level consumption [9,10]. The PhOH and their related compounds are extensively employed in industry to manufacture a variety of polymeric and drugs compounds such as rubber, fertilizer, paints, petroleum, pharmaceutical, and agricultural trades etc [9–11]. It's well documented that the PhOH is a carcinogenic compound and exposure resulted several symptoms for instance convulsions, dizziness and irregular respiration [9,12]. Besides this, some other phenols derivatives (eg. phenol, o-cresol, m-cresol, and p-cresol) are treated as atmospheric pollutants, whereas phenols are treated more toxic as water pollutants than as air pollutants [9]. This is often that the pollutant released from the industries as an industrial waste and arises in soil and drinking water supplies [13]. Although, their toxic effect, it's largely utilized as an essential compound for the beverages, fruit juices, wines [14,15], also exhibit bad and undesirable odor with highly toxic in nature for human health [16]. Therefore, it is required and urgent demand for the analysis of hazardous compounds at their trace level [17,18]. Because of the larger applicability of compounds in various directions, required qualitative and quantitative determination with various ways and also need to develop and determine the phenolic compounds. Towards this, the electrodes are significant components for the formation and determination of electrochemical analysis and also sensors formation. In the current scenario, the electrochemical analyses are largely applied for the determination of numerous analytes of interests in various environmental and medical applications [19]. Materials for electrodes must possess mixed electronic-ionic conductivity as well as electrocatalytic activity and obligatory to modify the electrodes with adding suitable electrocatalytic materials [20]. The features of electrodes for electrochemical detection can be well optimized through to their structure, material and the applied analyte to be detected. The electrochemical technique is simple, cost effective and provides rapid response, which offer high sensitivity, selectivity, reliability [21] and can play an important role in the detection and protection from the hazardous materials from the environment. The electrochemical sensors and detectors have the facility to detect and monitor on site for the priority pollutants; also can address other environmental requirements. These electrochemical devices are sensitive, selective, fast, accurate, compact, portable and inexpensive. Such type of arrangement in the electrochemical devices; facilitates and has significant impact for the decentralized and in clinical analysis. Hitherto, despite their great potential for the environmental monitoring, the electrochemical sensors for pollution control are still to their infancy stage. The current advancement in electrochemical sensor technology will definitely enlarge their scope of such type of devices for the detection, quantification and analysis of a series of organic and inorganic contaminants. The advances include ultra-micro electrodes (UME) of molecular devices (MD) or chemical and biological sensor arrays, micro-fabrication, computerized instrumentation and flow detectors etc. Several spectrophotometric and chromatographic techniques such as gas chromatography (GC), high performance liquid chromatography (HPLC), flow-injection analysis (FIA), capillary electrophoresis (CE) have been largely utilized [22–27]. Over a long range of applied chromatographic techniques for the separation and quantification of mixtures need various complex treatments for the analytical determination, whereas from the spectrophotometry the detection of colored polluted sample is complicated [28]. Out of these applied techniques, the electrochemical sensing provides the facility to analyse samples automatically, rapid detection, reliable and inexpensive measurements for a large number of pollutants. Considering the fact that selectivity and sensitive of electrochemical detection are strongly dependent on microstructures and properties of electrode materials, researchers are now focusing on the use of nanostructured materials or chemically modified electrodes [28–31]. The electrochemical detection technique provides a better platform to fabricate a robust sensor with high sensitivity, low-detection limit, good reproducibility and high durability. For the fabrication of electrochemical sensors, generally, artificial electron mediators are used, which help to transfer the electron from the electrode to the analyte. To this, number of materials were applied as an efficient electron mediator for the construction of electrochemical sensors. Over a past decade, it's found that the nanostructured materials exhibit good property such as high surface area, enhanced porosity etc; enable to transport electron in solution and electrode and work efficiently for various types of electrochemical sensors [32–36]. Among various nano and microstructured materials, the molybdenum oxides based nanostructures possess special place due to their excellent properties and wide applications [37–44]. The assembly of metal oxide nanostructures into ordered and perfect 2D & 3D superstructures has become an interesting aspect in sensors, catalysis etc [45–52]. The nanosized metal particles mediate the chemical reaction and provide better electro-catalytic activity in chemical sensor applications. From the past decade a number of innovate materials in a nano and micro scale have been synthesized via a wide range of green, chemical and physical methods. The exceptional properties for the nano and microstructures make them valued materials hence their enormous applicability in various fields such as photoelectric, catalysts, sensors, solar absorbers, energy etc [53–55]. The metal oxides nano materials are having a wide range of applications such as detection of catalysts, heavy metals, pathogens, organic and inorganic pollutants due to their special properties for instance high reactivity, enhanced specific surface area, optimized size distribution [53–55]. The oxides nanostructures have been shown to be highly efficient and active adsorbents for many toxic chemicals including air pollutants, chemical warfare agents, acidic gases, and water pollution [53–55]. Also serves as nanodevices, substrate for catalyst, sensor material [56–63]. The special property of metal oxide structures are credited to their excellent electron transfer and ultra-high surface area resulted from their nanoscale surfaces [64–67]. Towards this direction various types of nanocrystals including particles, rods, wires, cubes, octahedrons of noble metals have been synthesized and their catalytic properties were explored [68–70].

In a series of metal oxides nanostructures, the molybdenum oxide nano and micro structures exhibit larger band gap (2.8−3.6 eV) with vast applications in various directions such as batteries, optical and field emission devices, storage, solid lubricants, superconductors, photo chromic films, methanol oxidation, ionic conductors etc [71−73]. The MoO_3 is thermodynamically stable with different crystal phases (orthorhombic α-MoO_3, monoclinic β-MoO_3 and hexagonal h-MoO_3). Out of other phase the orthorhombic α-MoO_3 is highly anisotropic with layered structures stacked with bilayer of sheets bonded with van der Waals forces [74]. A number of ways were applied to form the molybdenum oxide nanostructures such as high temperature methods, thermal decomposition (TE), evaporation, PECVD, CVD, sonochemical, ultrasonic irradiation, hydrothermal and various other etc [74]. Out of these, the chemical or solution process is safe and cost effective to produced nano and micro structures in a bulk amount [75].

The present work described the formation of molybdenum nano and microstructures through chemical methods with using ammonium heptamolybdate tetrahydrate ($(NH_4)_6M o_7O_{24} 4H_2O)$) and sodium hydroxide. The synthesized powder was well characterized for to know their crystalline, structural and chemical characteristics. The formed molybdenum rod shaped structures assembled with nanosheets (α-MoO_3RANs) were applied on glassy carbon electrode (GCE), including platinum wire (counter electrode) and silver chloride (Ag/AgCl as reference electrode) for to sense the hazardous PhOH in liquid medium (PBS), opted various parameters such as effect of concentration, effect of potential, scan rates, chronoampherometric and electrochemical impedance (EIS) were measured with α-MoO_3RANs/ GCE electrode. Based on the acquired results and their discussions a mechanism was also presented.

2. Experimental

2.1. Material and methods

2.1.1. Synthesis of rod shaped molybdenum structures assembled with nanosheeets (α- α-MoO_3RANs)

The rods shaped assembles with nanosheets of molybdenum (α-MoO_3RANs) structures were produced via solution process with using ammonium heptamolybdate tetrahydrate ($(NH_4)_6M o_7O_{24}\cdot4H_2O)$) as a precursor material for rods shaped structures formation with NaOH. The entire chemicals such as $(NH_4)_6Mo_7O_{24}\cdot4H_2O$ and NaOH were purchased from Aldrich chemical corporation Co. U.S.A, received in Riyadh, Saudi Arabia and employed without any further purification. In a typical experiment: ammonium heptamolybdate tetrahydrate $(NH_4)_6 Mo_7O_{24}\cdot4H_2O$ (8 mM, ~0.93 g) and NaOH (0.3 M, ~1.2 g) were dissolved in double distilled water (DDW) and prepared solution separately. To this aqueous solution of ammonium heptamolybdate tetrahydrate, sodium hydroxide was added gradually in 100 mL of DDW under a uniform stirring condition and mixed well. The solutions pH was detected via pH meter (cole parmer, U.S.A) and it reached to 12.3. The solution was transferred in a refluxing pot and heated at 60 °C for 90 min. At initial, once the refluxing pot temperature rises the solution gets precipitates at the bottom of refluxing pot. The semi aqueous product was settled at the bottom of refluxing pot. After the complete refluxing process, the precipitated solution refluxing pot was cooled it at room for overnight. The product was transferred in a beaker and washed many times with solvents (alcohol, acetone etc) for to eliminate the scums in the solution. Further the product was washed through centrifugation (3000 rpm for 4 min) and desiccated to keep for other analysis.

2.1.2. Characterizations

The X-ray diffraction pattern (XRD) was used to know the processed powder particle size, phase and crystalline characteristics of the sample and analyzed from 10 to 60° with $Cu_{K\alpha}$ radiation (λ = 0.154 nm) at 6°/min scanning speed with an accelerating voltage of 40 kV and current of 30 mA. The structural detail of the powder was accessed through SEM at room temperature. To examine the SEM observation, the powder was consistently sprinkled on carbon tape which is pasted on sample holder. The sample holder was coated with powder and it transferred to the sputtering chamber for ~2−3 s to get the conducting layer on the surface of powder sample. Once the sample was sputtered, fixed it to SEM sample clamp and analyzed. For more clarification, the powder sample was further investigated through TEM (JEOL JEM-1011, Japan at 100 kV). For the observation, a pinch of synthesized powder was sonicated for ~10−15 min in an ethanol (EtOH) solvent with a 50 mL capacity beaker. Once the sonication was completed, a copper grid was inserted to this solution for ~2−3s and removes from the suspension solution and dried it at room temperature. The grid was fixed in a sample holder and analyzed the sample at room temperature. The functional detail of the processed material was examined through FTIR spectroscopy with using KBr pellets in the range from 400 to 4000 cm^{-1}. To analyse the FTIR spectroscopy, very small amount of sample was mixed with KBr powder and form a pellet with applying a high pressure (~4 ton (t)). The formed pellet was fixed with a sample holder of FTIR spectroscopy and examined.

2.2. α-MoO_3RANs based sensor for the detection of PhOH sensor

The processed powder of α-MoO_3 in the form of rod shaped structures with various nanosheets (α-MoO_3RANs) were utilized as an electroactive/working electrode to sense the PhOH in PBS (phosphate buffer saline, 0.1 M, PH = 7.2). The electrode was fabricated with the use of α-MoO_3RANs, coated as film form on GCE electrode (active surface area = 7 × 10^{-2} cm^2). The coating was performed with the use of very less amount of α-MoO_3RANs mixed it with the butyl carbitol acetate (BCA, specified ratio 75:25) and the semi liquidy α-MoO_3RANs solution was casted on GCE electrode, dried at 60±5 °C for 30−45 min to get a uniform layer over the entire GEC surface. The coated electrodes electrochemical study was run via autolab potentiostat/galvanostat, PGSTAT 204-FRA32 control with NOVA software (Metrohom Autolab B·V.Kanaalweg 29-G, 3526 KM Utrecht, Netherlands) in three electrode system [74,75]. The α-MoO_3RANs/GCE was employed as a working electrode, whereas a platinum (pt) wire was castoff as a counter electrode and Ag/AgCl (sat.KCl) was involved as a reference electrode. The PBS (0.1 M; pH 7.2) with PhOH was used as an electrolyte solution for the entire electrochemical measurements. For to sense PhOH conc. with α-MoO_3RANs/GCE, an inclusive range of PhOH (7.8 μM, 15.62 μM, 31.25 μM, 62.25 μM, 250 μM, 500 μM and 10 00 μM in PBS) with −1.5 to +1.5V current was adopted to determine the sensing evaluations. The potential data was examined with in a range from 5 to 100 mV of PhOH. The reproducibility of the processed sensor was checked at seven and 30 days reprehensive cycles. With this, the amperometry was also checked from 0 to 1500s of PhOH in PBS, the effect of impedance at different concentrations of PhOH (7.8 μM, 15.62 μM, 31.25 μM, 62.25 μM, 250 μM, 500 μM and 1000 μM) with current-time (i-t) curves were examined at a set potential in PBS solution.

3. Result and discussion

3.1. X-ray diffraction pattern (XRD results)

The procured powder crystalline property and their crystal phases were examined as described in material and method section

2.1.2. The XRD data shows several peaks obtained at a defined positions such as 12.5°, 23.14°, 25.34°, 27.15°, 33. 52°, 35.29°, 38.80°, 45.49°, 46.05°, 49.03°, 52.68°, 54.88° and 58.53° relate to the planes (020), (110), (040), (021), (111), (041), (060), (210), (002), (042), (211), (112) and (081) respectively. The XRD pattern shows peaks, which are very similar to the crystalline α-MoO$_3$, except any other impurities and matched with JCPDS data card no. 05−0508 with crystal lattice constants are a = 3.962 Å, b = 13.858 Å and c = 3.697 Å with orthorhombic structure. The X-ray diffraction pattern displayed the formation of α-MoO$_3$ nanostructures ((Fig. 1) [73,74].

3.2. Structural observations (SEM& TEM results)

Fig. 2. Show the low & high magnified images of processed structures of the prepared powder. The SEM analysis was employed for to know the structural detail of the powder sample. From the image (Fig. 2a shows that in a larger amount of rod shaped structures are seen and it covered the whole surface and it confirmed that the processed powder is in a large quantity. Fig. 2b also shows and confirms that the formation of rods shaped structures. The structural detail display of the recovered powder having an estimated magnitude of rod like structure with a diameter of ~2 μm and length goes up to ~6 μm. Once we have observed the images at higher magnification (Fig. 2c and d), it reveals that each rod is made up with several sheets like structures with ~200 nm in size. Some particles are jointed with each other; it appears that the sheets are in conjugation with other structures (Fig. 2c). The surface of each rod shaped structures are exhibit smooth and clean (Fig. 2 (d)). From the low and high magnified images, it shows that the sheets are stacked/combination and jointed with each other to form in a manner of rods shaped structures [73,74].

For to know the comprehensive detail of the prepared structure about the morphology of the formed powder material was further examined with TEM, as described in materials and methods (section 2.1.2). The TEM data exposed that the morphology of α-MoO$_3$RANs, which exhibited a similar result as obtained from SEM. From Fig. 3a and b, shows that the individual rods shaped structures exhibit 2 μm in diameter whereas length reached up to 6 μm. Each rod is having specified structures with smooth surfaces. From TEM image (Fig. 3), it is apparent that the rods shaped structures are made up with several sheets of nuclei and the acquired informations are consistent with the X-ray diffraction pattern (XRD) (Fig. 1) & SEM (Fig. 2) [73,74].
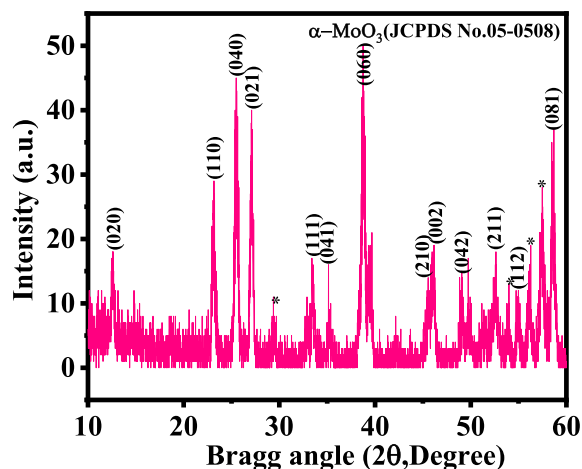

Fig. 1. X-ray diffraction of the prepared α-MoO$_3$ Nanorods, whereas the * shows the unidentified peaks.

3.3. FTIR spectroscopy of α-MoO$_3$RANs

The processed powders chemical/functional characteristics were evaluated through FTIR spectra and displayed as Fig. 4.The FTIR spectrum shows the fingerprints of ammonium heptamolybdate tetrahydrate ((NH$_4$)$_6$Mo$_7$O$_{24}$·4H$_2$O) and NaOH were used in the preparation of α-MoO$_3$. The broad and curved peak ranges from 3200 to 3600 cm^{-1} is corelated to the water molecule adsorbed on the surfaces whereas the asymetric striching of water molecules is associated at 1643 cm^{-1}. A small and pointed peak at 2364 cm^{-1} displayed for CO$_2$. The peak at 991 cm^{-1} is because of the stretching mode in Mo=O terminal oxygen, whereas at 875 cm^{-1} is related to the straching mode for the metal and oxygen bond (Mo−O−Mo). A semi and curved peak at around 540 cm^{-1} in FTIR spectrum represents the bending mode of vibration of O−Mo−O molecule [73−75]. The spectra depicts that the prepared rod shaped structures are having good chemical characteristics and justifies with XRD data.

3.4. Possible proposed growth mechanism of α-MoO$_3$RANs

For to investigate the growth mechanism of molybdenum oxide rods assembled with nanosheets (α-MoO$_3$RANs), a simple solution method was opted with using ammonium hepta-molybdate tetrahydrate ((NH$_4$)$_6$Mo$_7$O$_{24}$·4H$_2$O)) and sodium hydroxide (NaOH). The metal salt was dissolved in double distilled water and to this salt, sodium hydroxide was incorporated slowly and to make a uniform stirring condition and mixed well. Before the stirring of the solution, the solution looks transparent and no precipitate or any adduct was formed in the solution. Once the solutions stirred under sonication bath, a kind of flocculent product is generated in a beaker for a few seconds and disappeared. We may assume these are the initial nuclei for the formation of molybdenum oxide rods assembled with nanosheets (α-MoO$_3$RANs) formed in the beaker. The solution pH plays a curtail role in the formation of any nanostructures, as we have used the alkali sodium hydroxide in our experiment, the solution was measured to be 12.3. For the growth formation of nano or microstructures, it's required to provide the sufficient energy to solution or reaction. The aqueous solution was transferred to the refluxing pot and refluxed at 60 °C for 90 min. As observed from the refluxing pot no precipitate was formed initially. Once the refluxing pots temperature increases in a prolonged manner the growth of nuclei gets energized with heating temperature. The initial nuclei formed the base and side walls of the rods assembled sheet structure. As the refluxing temperature completed, the final structure of the nano or microstructures were received in an aqueous medium (as illustrated in Fig. 5) [73,76]. As stated in material and method the prepared structures were thoroughly washed with alcohol (methanol, ethanol etc) and acetone to purify the grown structures. In addition to this the structures were also centrifuged at 3000 rpm for 4 min to eliminate the ionic impurities from the solution structure. The product was room temperature dried to confirm the structural detail of the product. It's assumed that the geometry of rods assembled with nanosheets (RANs) like structures formed completely at this stage. The confirmation of the complete structure, phases and their crystalline property were confirmed from X-ray diffraction pattern and it reveals that the grown crystallite are α-MoO$_3$ structures, orthorhombic in nature with lattice constants are a = 3.962 Å, b = 13.858 Å and c = 3.697 Å. The final grown morphology of molybdenum oxide rods assembled with nanosheets (α-MoO$_3$RANs) was confirmed from the SEM, which reveals that the final formed structure are a combination of various nanosheets and stacked with each other. The size of each rod shaped structures is ~2 μm and length goes up to ~6 μm. The higher magnified images revels that
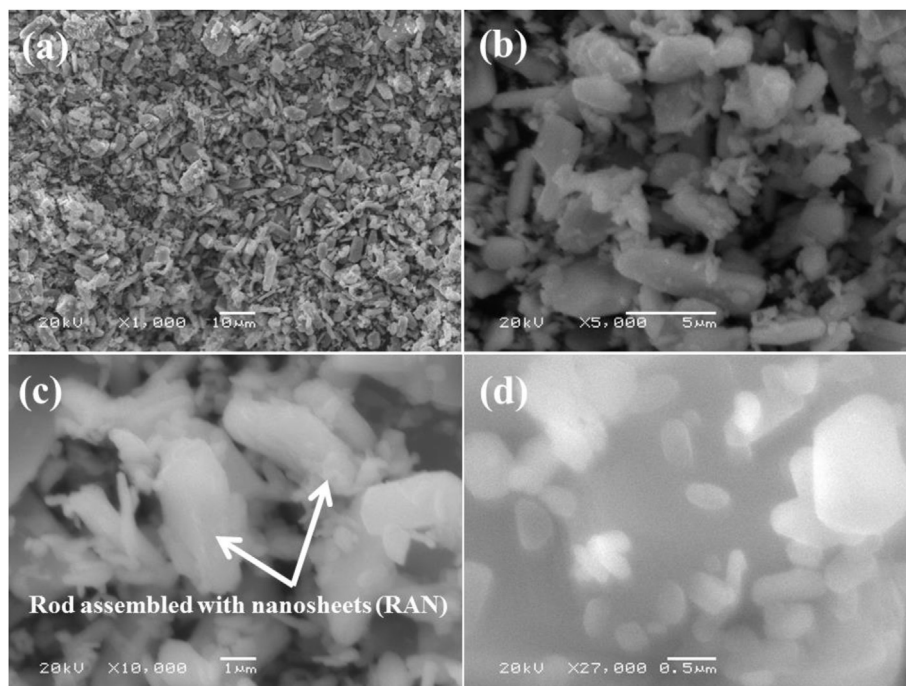
Fig. 2. SEM images of α-MoO₃ nanopowder: (a—b) apprehended at low magnification and (c—d) captured at high magnified scale.
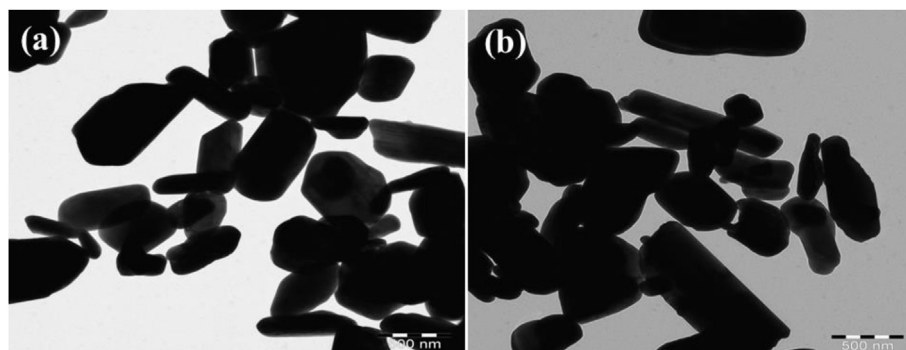

Fig. 3. Shows the TEM image of prepared α-MoO₃ nanorods (a) and (b) at different directions.

each rod is made up with several sheets like structures with ~200 nm in size. This was further confirmed from TEM, which also shows that the individual rods shaped structures exhibit 2 μm in diameter whereas length reached up to 6 μm. The FTIR spectroscopy, which is a chemical foot print of the processed material, also reveals the formation and represents the formation of α-MoO₃ RANs due to the presence of oxygen bond (Mo—O—Mo) [73,76].

3.5. Electrochemical/cyclic voltammetry (CV) studies with α-MoO₃RANs electrode

As described in the material and methods section 2.2, at initial on the top of the GCE electrode a film was made with the formed nanostructures and analyzed the coated (area 3 × 3 cm²) and noncoated electrode pasted on GCE. The modified electrode electrochemical characteristics were evaluated in terms of CV with the presence of PhOH (7.8 μM, 15.62 μM, 31.25 μM, 62.25 μM, 250 μM, 500 μM and 1000 μM) in 100 mL of PBS (0.1 M, pH 7.2) solution (scan rate 100 mV/s). When we have analyzed the bare electrode in

PhOH, it doesn't show any signal in the spectrum, which is very clear that no oxidation/reduction peak was observed and it depicts that there is no potential on bare electrode. Once the coated electrode α-MoO₃RANs/GCE were checked in presence of PhOH at 500 μM concentration, it show the enhanced activity for the PhOH oxidation [75]. As described from the obtained data, set potential and current (0.344, 2.56 × 10⁻⁴) for PhOH solution respectively [77] and its confirmed that the α-MoO₃RANs/GCE is efficient and to transport of the electron and oxidize the PhOH solution (Fig. 6) [77].

3.6. Effect of PhOH concentration on modified electrode (α-MoO₃RANs/GCE)

To know the change of current and potential (I–V) with modified α-MoO₃RANs/GCE, a series of concentration ranges from 7.8 μM, 15.62 μM, 31.25 μM, 62.25 μM, 250 μM, 500 μM and 1000 μM of PhOH in 100 mL PBS was acquired and the data is presented as Fig. 6. From the obtained graph it's revealed that a sequential change in oxidation and reduction peaks from a very low
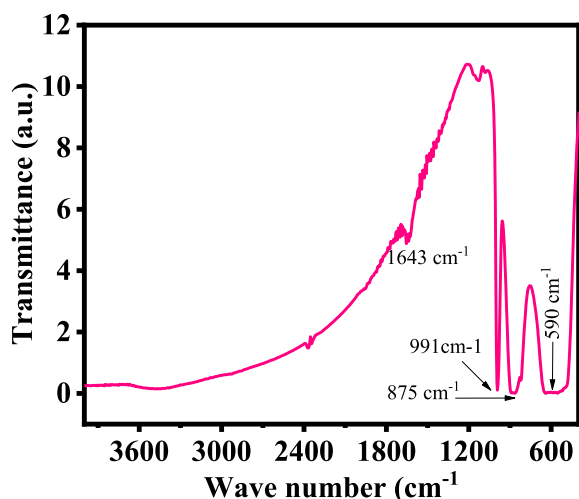
Fig. 4. FTIR spectrum of grown α-MoO₃ nanorods.

range of PhOH concentration solution with a high concentration solution was examined at 100 mV with current potential ranges from −1.5 to +1.5 V. As per the data (Fig. 7), illustrates that the current is directly proportional with PhOH concentration. Once the concentration of PhOH raises, the current in the form of ions increases and it help in the movement of electrons transfer at conduction band. A high potential of anodic peak was also observed from other cycles of experiments, when PhOH was used at high concentration level. It's postulated that the electron was displaced due to the increased amount of hydrogen ions in the solution and on also surfaces oxygen on the working electrode (Fig. 7).

3.7. Influence of potential at α-MoO₃RANs/GCE electrode

To know more detail related to the reliability of α-MoO₃RANs/GCE, a long range of potentials (10, 20, 30, 40, 50, 60, 70, 80, 90 and 100 mV/s) were opted and tested the sensing in PBS and the recovered result is presented as Fig. 8. A successive cathodic peak current of the modified electrode α-MoO₃RANs/GCE was observed with the increase of potential/scan rate from 10 to 100 mV/s which is a characteristic of electrode. The peaks of potential shifted positively at higher scan rate and negatively at lower scan rate,

respectively at different cycles of fixed concentration of PhOH in 0.1 M PBS solution at pH 7.2. It shows that the enhancement between the current and potential of α-MoO₃RANs/GCE for PhOH. At initial, a small anodic and cathodic peak was observed in the spectrum, illustrates that not enough potential was observed but when the parameters of potential changes, it can be clearly seen in the increase in current. This change attributes that the processed α-MoO₃RANs/GCE is functional and the material easily sense the PhOH in PBS solution. The obtained result implies the electrostatic interaction between the modified α- MoO₃RANs/GCE and PhOH are kinetically controlled by diffusion process [78−80]. As per the obtained results and their discussion related to the variation of concentration and potential, the linear plots were also constructed to know the ionization potential of cathode (IPc) and anode (IPa) also for the evaluation of correlation coefficient (R^2). The observations reveals that in both (IPa & IPc) for α-MoO₃RANs/GCE, the value of R^2 were 0.997 and 0.999 respectively (Fig. 9). Apart from this, the limit of detection (LOD) for α-MoO₃RANs/GCE (IPa) and α-MoO₃RANs/GCE (IPc) were evaluated which were 0.477 and 0.121 respectively. The limit of quantitation (LOQ) for α-MoO₃RANs/GCE (IPa) and α-MoO₃RANs/GCE (IPc) were evaluated which were 1.445 and 0.363 respectively (Table 1) [81].

3.8. Reproducibility and stability of the modified (α-MoO₃RANs/ GCE) electrode with consecutive cycle's response

The formed α-MoO₃RANs/GCE sensors reproducibility and stability were tested in terms of their of cycle response and the obtained data is presented as Fig. 10 (a & b). The tested data at different seven parallel reproducible cycles (Fig. 10a) and stability (Fig. 10 (b)), respectively of α-MoO₃RANs/GCE in presence of PhOH (62.25 μM) in 0.1 M PBS was observed. It shows that the excellent reproducibility for the consecutive measurements in presence of PhOH. The observation for reproducibility was tested from one to seventh days (Fig. 10a). In this time the sensor was kept in an ambient atmosphere, that's why it only shows a little change in the shape of cycle response. Further the stability of the processed α-MoO₃RANs/GCE sensor was again tested for a longer period (30 days) (Fig. 10b), which further confirm that the formed sensor is good and stable for long time interval. The data shows that the prepared electrode possessed highly satisfying, reproducible and sustainable for longer periods, useful to test for industrial samples [74,75,77−80].
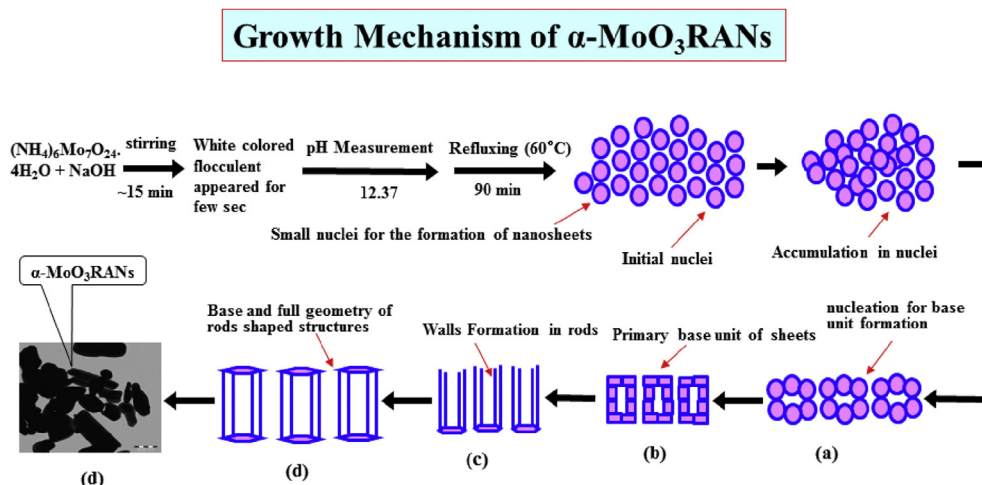

Fig. 5. Growth Mechanism of α-MoO₃RANs.

Table 1
Limit of detection (LOD) and Limit of quantification for α-MoO₃RANs/GCE.

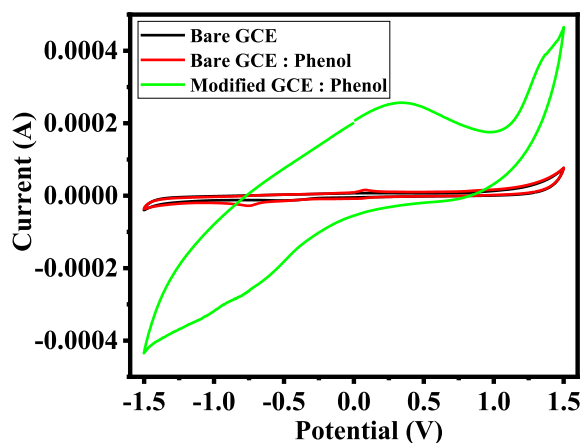| S.No	Metal Oxide	LOD (μM)	LOQ (μM)	Correlation coefficient (R^2)
1.	α-MoO₃RANs/GCE (IPa)	0.477	1.445	0.997
2.	α-MoO₃RANs/GCE (IPc)	0.121	0.363	0.999

Fig. 6. Cyclic voltammograms of bare and modified electrodes in the absence and presence of PhOH in 0.1M phosphate buffer (pH 7.2). Scan rate: 100 mVs^{-1}.

Fig. 8. Cyclic voltammetric responses of α-MoO₃RANs/GCE in the presence of PhOH (62. 25 μM) as a function of scan rates (a–j: 10, 20, 30, 40, 50, 60, 70, 80, 90 and 100 mV).

3.9. Influence of time response with α-MoO₃RANs/GCE against PhOH

The chronoamperometric curve is employed to access the activity and steadiness of the catalyst. A successive time response was observed from 0 to 1500 s for α-MoO₃RANs/GCE in PhOH for α-MoO₃RANs/GCE to evaluate the sensor selectivity and reproducibility (Fig. 11). A systematic change was examined at different time for the prepared α-MoO₃ RANs/GCE based PhOH sensor. The time response was observed in terms of current at different time interval such as at 36 s, 93 s, 203 s, 406 s, 771 s, 1021 s and 1243 s current improves to -2.29×10^{-4}, -6.39×10^{-5}, -2.63×10^{-4}, 1.40×10^{-4}, -5.63×10^{-4}, -5.28×10^{-5} and -4.46×10^{-5} respectively for α-MoO₃RANs/GCE electrode. The chronological and successive data showed that the sensor is specific, selective and reproducible. The time dependent and specific study for the
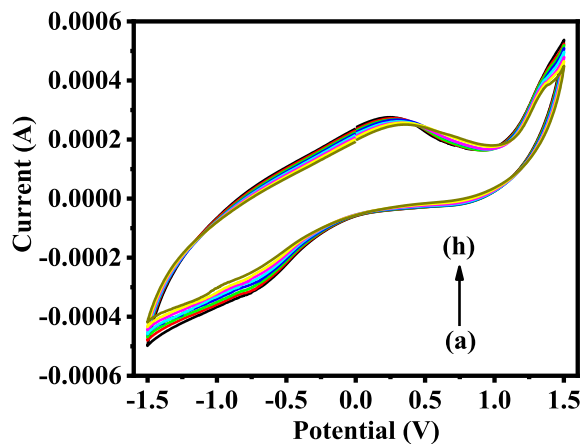
produced sensor has enough sustainability and reliability for period of time. The current−time response of chronoamperometric curve illustrates that once the potential increased, the current of electrode is reduced, which is indicated that the poisoning of catalyst by intermediate species during the reduction process [74,75,77−80].

3.10. Electrochemical impedance (EIS) for α-MoO₃RANs/GCE

The electrochemical impedance spectroscopy (EIS) is a technique to know the working electrode (α-MoO₃RANs/GCE) resistance and conductance of analyte. In this experiment a series of different concentrations (7.8 μM, 15.62 μM, 31.25 μM, 62.25 μM, 250 μM, 500 μM and 1000 μM in 100 mL PBS (0.1 M)) of PhOH was opted and analyzed in a frequency ranges from 0.01 to 10 kHz (Fig. 12). In this spectrum X-axis denotes the ohmic and Y axis display the capacitive property in the Nyquist plot. As per the

Fig. 7. Cyclic voltammetric responses of α-MoO₃RANs/GCE in 0.1 M phosphate buffer at different concentrations of PhOH (a–h: 7.8 μM, 15.62 μM, 31.25 μM, 62.25 μM, 250 μM, 500 μM and 1000 μM).
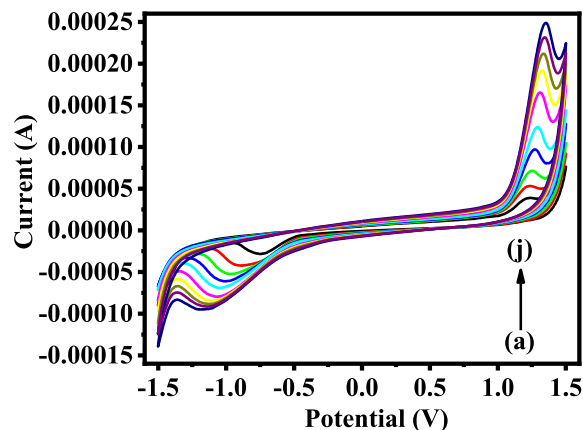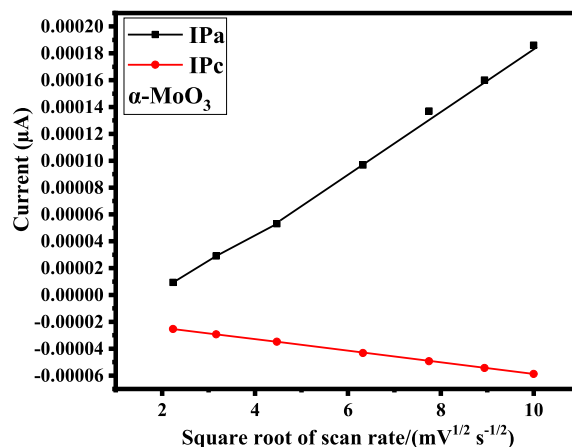

Fig. 9. Liner calibration graph for cathode and anode potentials of α-MoO₃RANs/GCE.
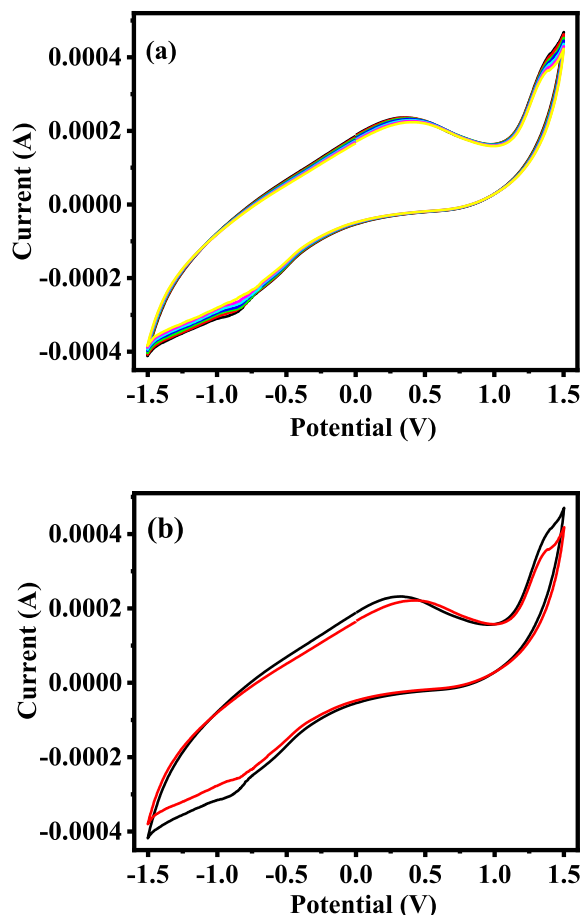
Fig. 10. (a). Seven consecutive cycles of α-MoO$_3$RANs/GCE in presence of 62.25 μM (PhO H) in 0.1 M PBS at 100 mV/s (b) Stability test first and after 30 days at the same conditions.

previous literature [82] and its well known that the impedance subjected from high to low frequency regions respectively. In present result showed many curves in semicircles shapes of EIS, represent that less charge transfer resistance received from the formed or modified α-MoO$_3$RANs/GCE. The curved spectra revels that the blank sample shows a state line, which depicts that less
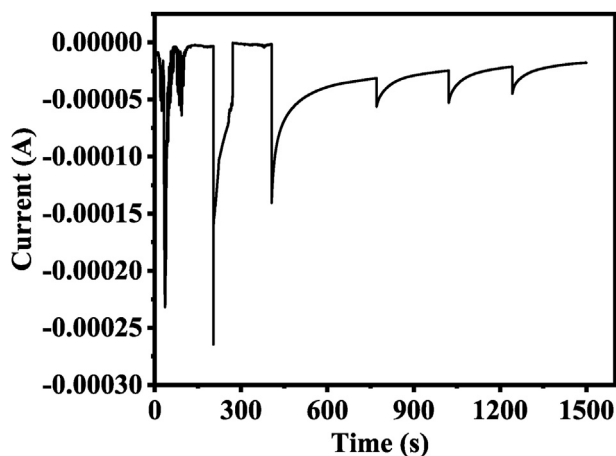

Fig. 11. Amperometric test for the α-MoO$_3$RANs/GCE by subsequent additions of in PhOH in 0.1 M PBS.
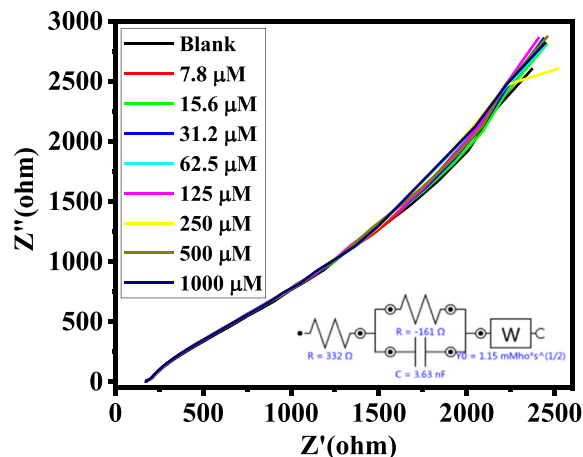

Fig. 12. Electrochemical impedance spectra of α-MoO$_3$RANs/GCE in 0.1 M PBS at different concentrations of PhOH (a−h: 7.8 μM, 15.62 μM, 31.25 μM, 62.25 μM, 250 μM, 500 μM and 1000 μM).

frequency with limited electron-transfer process but once the different concentrations of PhOH were used in the PBS and analyzed the EIS, many curved semicircle are in the high-frequency region was observed. This is analogous to electron-transfer at limited process. The diameter of each semicircle displays that the high frequency and resistance charge transfer ((Rct), and it's responsible to control the electron transfer rate at electrode interface. It is well-known fact that the larger the semicircle curve illustrates a high interfacial Rct, and resulted a poor electrical conductivity of the prepared/active materials. The results in the form of curves (Fig. 12) reveals that diameter of the semicircle at low PhOH concentrations are started and large in size, which is directly associated to the higher concentrations, this may be due to high Rct (Ω) values in the α-MoO$_3$RANs/GCE [82]. The semicircles diameter is increases with increase of concentration of PhOH, attributes that the Rct(Ω) value is analogous and directly proportional to the PhOH concentrations and that's why the α-MoO$_3$RANs having an active catalytic properties [80,82,83]. Also we have calculated the values of solution resistance (Rs(Ω)) and charge transfer resistance Rct(Ω) using circuit ((Fig. 12). The Rs and are Rct values gradually decrease while increasing the concentration of PhOH in PBS, which shows that the formed sensor is good and repeatable (Table 2). A plot was also constructed on the basis of the obtained values of solution resistance (Rs(Ω)) and charge transfer resistance Rct(Ω) to show the difference in EIS plots with increasing concentration of PhOH (Fig. 13).

3.11. Possible mechanism and discussion

The rods shaped molybdenum assembled with nanosheets (α-MoO$_3$RANs/GCE) like structures exhibit wide band gap (2.8−3.6 eV), n-type semiconductor with a captivating transition metal oxide material [74]. The α-MoO$_3$ is largely utilized in various fields of opto-electronic devices and sensors such as optical devices, storage, field emission devices etc [72−75,77]. In this work, the α-MoO$_3$ structures were synthesized through precipitation process as mentioned in section 2.1.1. The formed rod shaped structures assembled with various nanosheets (α-MoO$_3$RANs) were characterized with various techniques as described in section 2.1.2 for occurrence of XRD, SEM, TEM and FTIR spectroscopy to know the crystallinity, structural and chemical characteristic of the material. The well characterized material was utilized as a sensor material

Table 2
Shows the solution resistance (RS(Ω)) and charge transfer resistance RCt(Ω) for the PhOH.

Code (Concentration μM))	RS(Ω)	RCt(Ω)
Blank	332	−161
7.8	277	−2.44
15.6	263	−2.80
31.25	171	−5.41
62.5	170	−5.47
125	169	−5.64
250	167	−6.01
500	166	−6.10
1000	117	−6.34
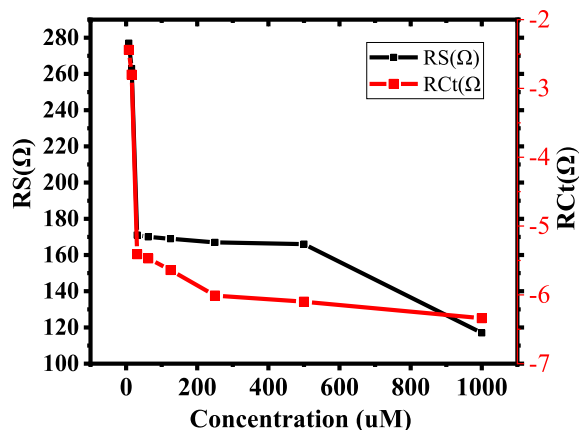
Fig. 13. Effect of solution resistance (Rs(Ω)) and charge transfer resistance Rct(Ω) with incr-easing concentration of PhOH.

and a film coated on GCE, which was made it as working electrode, to evaluate their electrical and sensing property. The PhOH is a toxic industrial chemical and it requires and an urgent demand to check their sensing characteristic through low cost and effective process. To keep this point, in this experiment, we have opted a long range of PhOH concentrations (7.8 μM, 15.62 μM, 31.25 μM, 62.25 μM, 250 μM, 500 μM and 1000 μM/100 mL in PBS (0.1 M)) via prepared working electrode (α-MoO$_3$RANs/GCE) detection via electrochemical method. The prepared working electrode (α-MoO$_3$RAN s/ GCE) plays an important role in electron transportation process. As per the received data (cell cycles and reproducibility data) higher and longer period stability and reproducibility of α-MoO$_3$RANs/GCE electrode can facilitates for the large scale industrial and environmental samples detection of PhOH. The developed α-MoO$_3$RANs/ GCE electrode works on varied concentration of analyte (PhOH), their adsorption and conductance were completed on α-MoO$_3$R-ANs/GCE surfaces. As described in material and method section, once the α-MoO$_3$ rods assembled with various nanosheets were mixed in an organic adhesive and to form a slurry. The formed slurry was coated on GCE to a form a thick layer and dried well. The well dried GCE was immersed in PBS and checked the electrochemical examination at a varied concentration of analyte (PhOH). It's postulated that the surface of the prepared electrode α-MoO$_3$RANs/GCE have possibility to trap the atmospheric oxygen, adsorb on the surfaces and this trapped oxygen interchange and further ionized (O$^-$$_{ads}$) via the removal of electron as the conduction band and it convert into oxidized (O$^-$ or O^{2-}) form on surface layer of α-MoO$_3$RANs/GCE. This conductance and interchange of surfaces oxygen form a charged layer between the electrode (α-MoO$_3$RANs/GCE) and analyte [84,85]. The surface adsorb oxygen has capability to amplifies the potential of the prepared electrode,

which improved the resistance in the processed assembly. The experiment leads a reduction in conductance and increase in potential of the formed (α-MoO$_3$RANs/GEC) electrode. From this experiment, it reveals that a crucial change in concentrations from low to high of analyte (PhOH) delivers a higher efficiency of the electrode. The data received from the experiments also influences with various basic parameters such as architecture of nanostructured materials (rods, flowers, tubes, wires, belts etc), pH of the solution, used electrolyte, chemical properties of the used materials, surface properties of electrodes etc. Because the rods shaped structures is made up of several tiny nanosheets (~200 nm size), which have high surface properties as compared to other shaped nanostructures. The tiny nanosheets facilitates the increased band gap and generates high electron transportation also provides good sensing capacity. The α-MoO$_3$RANs provides a good affinity towards the surface of GCE and it produces feasible environment to their surfaces also provides passages to react with the analyte via surface adsorption. The semiconductor materials exhibit stable and reproducible properties which authenticated good electron transportation between electrode film (α-MoO$_3$R-ANs) and analyte (PhOH). In addition to this, the surface adhesion of processed nano and micro-structures creates a bonding with analyte, which directly affects the reaction/response time, electrical signals, and enactment of the produced sensor. The formed α-MoO$_3$RANs/GCE surface also enhanced the catalyst (PhOH) with using a smooth and glassy film of electrode. In this experiment the PhOH plays an important role as a analyte to enhance the reaction with the surface adsorbed oxygen on film/layer (α-MoO$_3$RANs/ GCE), and thus it increases the conductance of the α-MoO$_3$RANs/ GCE [84,85]. The semiconductors nano or microstructures which have various sheets like structures enbuild, facilitates a number of routes for the surface adsorption of analyte (PhOH), leads to a significant transportation of electrons between the electrode film (α-MoO$_3$RANs/GCE) and solution (PhOH in PBS) (Fig. 12). The charge transfer resistance RCt(Ω) values also signify that as the resistance circuit (RS(Ω)) decreases with the increase of concentration of PhOH, the current of the processed sensor increases, which is reproducible and repeatable for a longer period [82,86].

4. Conclusions

The summary of the present work states that the rods of molybdenum oxide assembled with nanosheets (α-MoO$_3$RANs) were formed with chemical/precipitation process. The chemical such as ammonium heptamolybdate tetrahydrate ((NH$_4$)$_6$Mo$_7$O$_{24}$·4H$_2$O)) and NaOH in a less time period (90 min) of heating at 60 °C. The prepared powder was well characterized in terms of their powder crystalline property, morphological study and electrochemical evaluation in detail. For this, initially the synthesized α-MoO$_3$R-ANSs was characterized through XRD to ascertain the crystallinity of the material whereas the morphology was recovered from SEM and it revealed that the individual rod shaped structures staked with many sheets (~200 nm) with diameter is 2 μm in and length reached to 6 μm. The structural detail was again confirmed via SEM and its corresponding with TEM results. The prepared powders chemical/functional characteristics were examined via FTIR spectroscopy. Based on the analysis and their observations a possible growth mechanism for the α-MoO$_3$RANs has been proposed and discussed. The formed α-MoO$_3$RANs /GCE was applied to sense the hazardous chemical compound of PhOH. The CV shows the cathodic and anodic signal in a liquid medium with PBS from a very range of electrolyte (7.8 μM−1000 μM in PhOH/100 mL) solution. It reveals from the obtained data that a concise change was observed in cathodic and anodic peaks, which depicts that the formed sensor is precise and it's useful for the detection of bulk samples. From the

observed selectivity and reproducibility (0−1500 *s*) data it expresses that the produced sensors exhibit abundant sustainability for longer period.

Data availability

The raw/processed data required to reproduce these findings cannot be shared at this time due to technical or time limitations.

Declaration of competing interest

The authors declare that they have no known competing financial interests or personal relationships that could have appeared to influence the work reported in this paper.

Acknowledgement

References

[1] M.M. Rahman, A.M. Asiri, Fabrication of highly sensitive ethanol sensor based on doped nanostructure materials using tiny chips, RSC Adv. 5 (2015) 63252−63263.

[2] J.Q. Xu, J.J. Han, Y. Zhang, Y.A. Sun, B. Xie, Studies on alcohol sensing mechanism of ZnO based gas sensors, Sensor. Actuator. B Chem. 132 (2008) 334−339.

[3] A. Sharma, N. Sharma, A. Kumari, H.J. Lee, T.Y. Kim, K.M. Tripathi, Nano-carbon based sensors for bacterial detection and discrimination in clinical diagnosis: a junction between material science and biology, Appl. Mater. Today 18 (2020) 100467.

[4] K.M. Tripathi, T.Y. Kim, D. Losic, T.T. Tung, Recent advances in engineered graphene and composites for detection of volatile organic compounds (VOCs) and non-invasive diseases diagnosis, Carbon 110 (2016) 97−129.

[5] R. Malik, V.K. Tomer, Y.K. Mishra, L. Lin, Functional gas sensing nano materials: a panoramic view, Appl. Phys. Rev. 7 (2020), 021301, https://doi.org/10.1063/1.5123479.

[6] K. Yu, A. Xin, H. Du, Y. Li, Q. Wang, Additive Manufacturing of Self-Healing Elastomers 11, vol. 7, 2019, https://doi.org/10.1038/s41427-019-0109-y.

[7] S. Ammar, N. Oturan, M.A. Oturan, Electrochemical oxidation of 2-nitrophenol in aqueous medium by electro-fenton technology, J. Environ. Eng. Manage 17 (2007) 89−96.

[8] R.S. Ribeiro, A.M.T. Silva, J.L. Figueiredo, J.L. Faria, Removal of 2-nitrophenol by catalytic wet peroxide oxidation using carbon materials with different morphological and chemical properties, Appl. Catal. B Environ. 140−141 (2013) 356−362.

[9] F.A. Patty, Industrial Hygiene and Toxicology, vol. 2, Interscience, New York, 1963, p. 1363.

[10] I.M. Kolthoff, P.J. Elving, F.H. Stross, Treatise on Analytical Chemistry, vol. 2, Wiley, New York, 1971, p. 490.

[11] W. Leithe, Analysis of Air Pollutants, Ann Arbor Science, Ann Arbor, MI, 1971, p. 246.

[12] W. Leithe, Analysis of Organic Pollutants in Water and Waste Water, Ann Arbor Science, Ann Arbor, MI, 1972, p. 113.

[13] S.E. Manahan, Fundamental of Environmental Chemistry, Lewis, Boca Raton, 1993, p. 618.

[14] A. Morales, D.A. Birkholz, S.E. Hrudey, Analysis of pulp mill effluent contaminations in water, sediment and fish bile fatty and resin acids, Water Environ. Res. 64 (1992) 660−666.

[15] G.K. Buckee, Determination of the volatile components of beer, J. Inst. Brew. 98 (2) (1992) 78−79.

[16] D. Chen, A.K. Ray, Photodegradation kinetics of 4-nitrophenol in TiO₂ suspension, Water Res. 32 (1998) 3223−3234.

[17] P.A. Realini, Determination of priority pollutant phenols in water by HPLC, J.Chrom. Sci. 19 (1981) 124−129.

[18] R. Tyagi, Determination of substituted phenols in water by gas chromatography/mass spectroscopy after solid phase extraction, Fresenius Environ. Bull. 4 (1995) 751−759.

[19] E. Bakker, Y. Qin, Electrochemical sensors, Anal. Chem. 78 (2006) 3965−3984.

[20] U. Guth, J. Zosel, J. Riedel, N. Tran, M. Berthold, C. Vonau, U. Sasum, P. Shuk, M. Paramasivam, V. Vashook, Novel electrode materials for electrochemical sensors, Sensing Technology (ICST), in: Fifth International Conference on IEEE, 2011, pp. 685−689.

[21] S.K. Kim, Y.N. Jeong, M.S. Ahmed, J.M. You, H.C. Choi, S. Jeon, Electrocatalytic deter- mination of hydrazine by a glassy carbon electrode modified with PEDOP/MWCNTs −Pd nanoparticles, Sens. Actuators, B 153 (2011) 246−251.

[22] X. Guo, Z. Wang, S. Zhou, The separation and determination of nitrophenol isomers by high-performance capillary zone electrophoresis, Talanta 64 (2004) 135−139.

[23] M. Miro, A. Cladera, J.M. Estela, V. Cerda, Dual wetting-film multi-syringe flow inject- ion analysis extraction: application to the simultaneous determination of nitro phenols, Anal. Chim. Acta 438 (2001) 103−116.

[24] E. Tesarova, D. Sykora, Z. Voznakova, GC and HPLC determination of nitrophenol related pesticides, Fresenius Environ. Bull. 4 (1995) 609−616.

[25] T. Zhao, T.X. Hu, J. Cheng, X. Lu, Use of calix[4]arene to separate positional isomers in capillary electrophoresis, Anal. Chim. Acta 358 (1998) 263−268.

[26] C.H. Yang, Electrochemical determination of 4-nitrophenol using a single-wall car- bon nanotube film-coated glassy carbon electrode, Microchim.Acta 148 (2004) 87−92.

[27] F. Elbarbry, K. Wilby, J. Alcorn, Validation of a HPLC method for the determination of p-nitrophenol hydroxylase activity in rat hepatic microsomes, J.Chrom.B 834 (2006) 199−203.

[28] H.S. Yin, Y.L. Zhou, S.Y. Ai, X. Liu, L. Zhu, L. Lu, Electrochemical oxidative determi-nation of 4-nitrophenol based on a glassy carbon electrode modified with a hydro- xyapatite nanopowder, Microchim Acta 169 (2010) 87−92.

[29] H. Li, S. Liu, Z. Dai, J. Bao, X. Yang, Applications of nanomaterials in electrochemical enzyme biosensors, Sensors 9 (11) (2009) 8547−8561.

[30] F. Xiao, L. Wang, H. Duan, Nanomaterial based electrochemical sensors for in vitro detection of small molecule metabolites, Biotechnol. Adv. 34 (3) (2016) 234−249.

[31] C. Zhu, G. Yang, H. Li, D. Du, Y. Lin, Electrochemical sensors and biosensors based on nanomaterials and nanostructures, Anal. Chem. 87 (1) (2015) 230−249.

[32] A. Umar, Y.B. Hahn, in: Metal Oxide Nanostructures and Their Applications, vol. 5, American Sci. Publishers, USA, 2010, p. 4. S.Amlathe and V.K.Gupta, Analyst 113 (1988) 1481.

[33] S. Garrod, M.E. Bollard, A.W. Nicholls, S.C. Connor, J. Connelly, J.K. Nicholson, E. Holmes, Integrated metabonomic analysis of the multiorgan effects of hydrazine toxicity in the rat, Chem. Res. Toxicol. 18 (2) (2005) 115−122.

[34] J.W. Mo, B. Ogorevc, X. Zhang, B. Pihlar, Cobalt and copper hexacyanoferrate modified carbon fiber microelectrode as an all-solid potentiometric microsensor for hydrazine, Electroanalysis 12 (2000) 48−54.

[35] A. Safavi, A.A. Ensafi, Kinetic spectrophotometric determination of hydrazine, Anal. Chim. Acta 300 (1995) 307−311.

[36] S.M. Golabi, H.R. Zare, Electrocatalytic oxidation of hydrazine at glassy carbon elec trode modified with electrodeposited film derived from caffeic acid, Electroanalysis 11 (1999) 1293−1300.

[37] F. Caruso, R.A. Caruso, H. Möhwald, Nanoengineering of inorganic and hybrid hollow spheres by colloidal templating, Science 282 (1998) 1111−1114.

[38] I.W. Hamley, Nanostructure fabrication using block copolymers, Nanotechnology 14 (2003) 39−41.

[39] Y. Ding, P.X. Gao, Z.L. Wang, Catalyst− nanostructure interfacial lattice mismatch in determining the shape of VLS grown nanowires and nanobelts: a case of Sn/ZnO, J. Am. Chem. Soc. 126 (2004) 2066−2072.

[40] B. Wang, W. Feng, M. Zhu, Y. Wang, M. Wang, Neurotoxicity of low-dose repeatedly intranasal instillation of nano and submicron-sized ferric oxide particles in mice, J. Nanoparticle Res. 11 (2009) 41−53.

[41] W. Schartl, Crosslinked spherical nanoparticles with core−shell topology, Adv. Mat. 12 (2000) 1899−1908.

[42] X. Wang, J. Zhang, Q. Peng, Y.D. Li, A general strategy for nanocrystal synthesis, Nature 437 (2005) 121−124.

[43] D.B. Yu, V.W. Yam, Controlled synthesis of monodisperse silver nanocubes in water, J. Am. Chem. Soc. 126 (2004) 13200−13201.

[44] C. Hofmann, I. Rusakova, T. Ould-Ely, D. Prieto-Centurion, K.B. Hartman, A.T. Kelly, A. Luttge, K.H. Whitmire, Shape control of new FexO−Fe₃O₄ and Fe₁−yMnyO−Fe₃− zMnzO₄ nanostructures, Adv. Funct. Mater. 18 (2008) 1661−1667.

[45] P. Ball, Small problems, Nature 362 (1993) 123.

[46] S. Peschel, G. Schmid, First steps towards ordered monolayers of ligand-stabilized gold clusters, Angew Chem. Int. Ed. Engl. 34 (1995) 1442−1443.

[47] R.P. Andres, J.D. Bielefeld, J.I. Henderson, D.B. Janes, V.R. Kolagunta, C.P. Kubiak, W. Manoney, R.G. Osifchin, Science 273 (1996) 1690−1693.

[48] S. Hrapovic, J.H.T. Luong, Picoamperometric detection of glucose at ultrasmall platinum-based Biosensors: preparation and characterization, Anal. Chem. 75 (2003) 3308−3315.

[49] K.B. Male, S. Hrapovic, Y. Liu, D. Wang, J.H.T. Luong, Electrochemical detection of carbohydrates using copper nanoparticles and carbon nanotubes, Anal. Chim. Acta 516 (2004) 35−41.

[50] L.N. Lewis, Chemical catalysis by colloids and clusters, Chem. Rev. 93 (1993) 2693−2730.

[51] G.L. Cho, B.B. Lakshmi, E.R. Fischer, C.R. Martin, Implementation of a quantum search algorithm on a quantum computer, Nature 393 (1998) 344−346.

[52] J. Pei, X.Y. Li, Preparation, characterization and application of an electrode modified with electropolymerized CuPtCl₆, J. Electroanal. Chem. 441 (1998) 245−258.

[53] H. Chang, C. Lo, L.C. Chen, T.T. Tsung, C.S. Jwo, Photodecomposition and surface adsorption of methylene blue on TiO₂ nanofluid prepared by ASNSS, Mater. Trans. 45 (2004) 3334−3337.

[54] S. Rehman, Size effects on the magnetic and optical properties of CuO nanoparticles, J. Nanopart. Res. 13 (2011) 2497−2507.

[55] E Christian, Selective synthesis of clinoatacamite $Cu_2(OH)_3Cl$ and tenorite CuO nanoparticles by pH control, J. Nanoparticle Res. 16 (2014) 25−56.

[56] L. Phelane, F.N. Muya, H.L. Richards, P.G.L. Baker, E.I. Iwuoha, Polysulfone nano composite membranes with improved hydrophilicity, Electrochim. Acta 128 (2014) 326−335.

[57] M.L. Yola, N. Atar, Z. Üstündag, A.O. Solak, A novel voltammetric sensor based on p- aminothiophenol functionalized graphene oxide/gold nanoparticles for determining quercetin in the presence of ascorbic acid, J. Electroanal. Chem. 698 (2013) 9−16.

[58] M.L. Yola, N. Atar, T. Eren, H. Karimi-Maleh, S. Wang, Sensitive and selective determi- nation of aqueous triclosan based on gold nanoparticles on poly-oxometalate/reduced graphene oxide nanohybrid, RSC Adv. 5 (2015) 65953−65962.

[59] N. Atar, T. Eren, M.L. Yola, H. Karimi-Maleh, B. Demirdögen, Magnetic iron oxide and iron oxide@gold nanoparticle anchored nitrogen and sulfur-functionalized reduced graphene oxide electrocatalyst for methanol oxida-tion, RSC Adv. 5 (2015) 26402−26426, 409.

[60] F. Lorestani, P.M. Nia, Y. Alias, N.S.A. Manan, One-step synthesis of different silver- polyaniline composite morphologies for enzymless hydrogenper oxide detection, J. Electrochem. Soc. 162 (2015). B193−B200.

[61] G. Shen, P.C. Chen, K. Ryu, C. Zhou, Devices and chemical sensing applications of metal oxide nanowires, J. Mater. Chem. 19 (2009) 828−839.

[62] M. Chandra, Q. Xu, Room temperature hydrogen generation from aqueous ammonia- borane using noble metal nano-clusters as highly active catalysts, J. Power Sources 168 (2007) 135−142.

[63] O.K. Varghese, C. Grimes, Metal oxide nanoarchitectures for environmental sensing, J. Nanosci. Nanotechnol. 3 (2003) 277−293.

[64] C.N.R. Rao, G.U. Kulkarni, A. Govindaraj, B.C. Satishkumar, P.J. Thomas, Metal nano particles, nanowires, and carbon nanotubes, Pure Appl. Chem. 72 (1−2) (2000) 21−33.

[65] P.M. Nia, W.P. Meng, Y. Alias, Hydrogen peroxide sensor: uniformly decorated silver nanoparticles on polypyrrole for wide detection range, Appl. Surf. Sci. 357 (2015) 1565−1572.

[66] M. Okumura, T. Akita, M. Haruta, X. Wang, O. Kajikawa, O. Okada, Multi-component noble metal catalysts prepared by sequential deposition precipi-tation for low temp erature decomposition of dioxin, Appl. Catal. B Environ. 41 (2003) 43−52.

[67] A. Tolga Cᵒolak, T. Eren, M.L. Yola, E. Bes› li, O. S› ahin, N. Atar, 3Dpolyoxo metalate-functionalized graphene quantum dots with mono- Metallicand Bi-Metallic nanoparticles for application in direct methanol fuel cells, J. Electrochem. Soc. 163 (2016) F1237−F1244.

[68] B. Wiley, Y. Sun, Y. Xia, Synthesis of silver nanostructures with controlled shapes and properties, Acc. Chem. Res. 40 (2007) 1067−1076.

[69] M.L. Yola, N. Atar, Functionalized graphene quantum dots with Bi-Metallic nano particles composite: sensor application for simultaneous determina-tion of ascorbic acid, dopamine, uric acid and tryptophan, J. Electrochem. Soc. 163 (2016) B718−B725.

[70] S. Xu, S. Jiang, J. Wang, J. Wei, W. Yue, Y. Ma, Graphene isolated Au nano-particle arrays with high reproducibility for high-performance surface-enhanced Raman scattering, Sensor. Actuator. B Chem. 222 (2016) 1175−1183.

[71] L. Cai, P.M. Rao, X. Zheng, Morphology controlled flame synthesis of single, branched, and flower-like a-MoO3 nanobelts arrays, Nano Lett. 11 (2011) 872−877.

[72] D. Parviz, M. Kazemeini, A.M. Rashidi, K.J. Jozani, Synthesis and character-ization of MoO_3 nanostructures by solution combustion method employing morphology and size control, J. Nanoparticle Res. 12 (2010) 1509−1521.

[73] H. Hu, C. Deng, J. Xu, K. Zhang, M. Sun, Metastable h-MoO_3 and stable α-MoO_3 microstructures: controllable synthesis, growth mechanism and their enhanced photocatalytic activity, J. Exp. Nanosci. 10 (17) (2015) 1336−1346, https://doi.org/10.1080/17458080.2015.1012654.

[74] J.C. Park, H. Song, Synthesis of polycrystalline Mo/MoOx nanoflakes and their transformation to MoO3 and MoS2 nanoparticles, Chem. Mater. 19 (11) (2007) 2706−2708.

[75] L. Seguin, M. Figlarz, R. Cavagnat, J.C. Lasseguies, Infrared and Raman spectra of MoO_3 molybdenum trioxides and $MoO_3.xH_2O$ molybdenum trioxide hy-drates, Spectrochim. Acta, Part A 51 (1995) 1323−1344.

[76] J. Li, P. Wei, J. Chen, L. Rongti, Preparation and growth mechanism of mo-lybdenum trioxide whisker, J. Am. Ceram. Soc. 85 (8) (2002) 2116−2118.

[77] İ. Çakar, K.V. Özdokur, B. Demir, E. Yavuz, D.O. Demirkol, S. Koçak, S. Timur, F.N. Ertaş, Molybdenum oxide/platinum modified glassy carbon electrode: a novel electrocatalytic platform for the monitoring of electrochemical reduc-tion of oxygen and its biosensing applications, Sensor. Actuator. B Chem. 185 (2013) 331−336.

[78] E. Fazio, S. Spadaro, M. Bonsignore, N. Lavanya, C. Sekar, S.G. Leonardi, G. Neri, F. Neri, Molybdenum oxide nanoparticles for the sensitive and selective detection of Dopamine, J. Electroanal. Chem. 814 (2018) 91−96.

[79] K. Giribabu, R. Suresh, R. Manigandan, S. Munusamy, S.P. Kumar, S. Muthamizh, V. Narayanan, Nanomolar determination of 4-nitrophenol based on a poly (methylene blue) modified glassy carbon electrode, Analyst 138 (2013) 5811−5818.

[80] R. Cao, Q.C. Zhuang, L.L. Tian, X.Y. Qiu, Y.L. Shi, Electrochemical impedance spectroscopic study of the lithium storage mechanism in commercial mo-lybdenum disulfide, Ionics 20 (2014) 459−469.

[81] International organization for standardization accuracy (trueness and preci-sion) of measurement methods and results 5725, ISO/DIS, 1994.

[82] R.A. Nyquist, R.O. Kagel, Infrared Spectra of Inorganic Compounds, Academic Press, Inc, New York, London, 1971.

[83] R.S. Datta, F. Haque, M. Mohiuddin, B.J. Carey, N. Syed, A. Zavabeti, B. Zhang, H. Khan, K.J. Berean, J.Z. Ou, N. Mahmood, T. Daeneke, K. Kalantar-zadeh, Highly active two dimensional α-$MoO_{3−x}$ for the electrocatalytic hydrogen evolution reaction, J. Mater. Chem. 5 (2017) 24223−24231.

[84] S.G. Ansari, Z.A. Ansari, R. Wahab, Y.S. Kim, G. Khang, H.S. Shin, Glucose sensor based on nano-baskets of tin oxide templated in porous alumina by plasma enhanced CVD, Biosens. Bioelectron. 23 (2008) 1838−1842.

[85] H. Farahani, R. Wagiran, M.N. Hamidon, Humidity sensors principle, mecha-nism, and fabrication technologies: a comprehensive review, Sensors 14 (2014) 7881−7939, https://doi.org/10.3390/s140507881.

[86] R.N. Mariammal, K. Ramachandran, Study on gas sensing mechanism in p-CuO/n-ZnO heterojunction sensor, Mater. Res. Bull. 100 (2018) 420−428.